Inorg. Chem. **2008**, *47*, 8188−8196

Vibronic Effects in Cu(II)-Doped $Ba_2Zn(HCO_2)_6 \cdot 4H_2O$

Kieran S. Hadler,[†] James R. Kilmartin,[†] Graeme R. Hanson,[‡] Michael A. Hitchman,[§] Charles J. Simmons,[||] and Mark J. Riley*,[†]

School of Molecular and Microbial Science, University of Queensland, St. Lucia, QLD, 4072, Australia, Centre for Magnetic Resonance, University of Queensland, St. Lucia, QLD, 4072, Australia, School of Chemistry, University of Tasmania, Box 252-75 Hobart, TAS 7001, Australia, and Division of Natural Sciences, University of Hawaii, Hilo, Hawaii 96720-4091

Received April 22, 2008

The temperature-dependent electron paramagnetic resonance (EPR) spectrum of ∼1% Cu(II) ions doped into $Ba_2Zn(HCO_2)_6 \cdot 4H_2O$ was analyzed at the Q-band frequencies over the temperature range 100−350 K to obtain structural information about the local environment. It can be concluded that the host crystal imparts a large orthorhombic strain which mainly corresponds to a tetragonal compression imposed onto the $Cu^{II}O_6$ species. This results in a copper center which adopts an orthorhombically distorted elongated geometry with the elongated axis perpendicular to the direction of the tetragonal compression due to the host crystal. There are two possible axes of elongation, and these represent two conformers separated by ∼320 cm^{-1}. The thermal population of the higher energy level averages the *g* values, giving the observed temperature-dependent EPR spectra. The averaging process is between vibronic levels that are localized at two different minima of a *single* ground-state potential energy surface. These vibronic levels correspond to vibrational levels having different electronic properties. The determination of the host lattice strain parameters from the Cu(II) EPR spectra means that the guest ion is used as a probe of the environment of the Zn(II) site. The structural data derived from the lattice strain parameters are correlated with those from the $Ba_2Zn(HCO_2)_6 \cdot 4H_2O$ crystal structure.

Introduction

Many Jahn−Teller (JT) distorted six-coordinate copper(II) complexes appear to change their bond lengths as a function of the temperature, and the mechanisms by which this happens require knowledge of the ground-state potential energy surface.[1] The ^2E_g ground state of octahedral copper(II) is subject to a Jahn−Teller distortion, and early work on the E⊗e Jahn−Teller problem established the form of the vibronic Hamiltonian,[2] the numerical approach for its solution,[3] and the importance of higher-order terms in determining the stationary points in the potential energy surface.[4] It was also realized that, in the solid state, lower symmetry perturbations can have a large effect on the experimental observables, and the effects of lattice strain were incorporated into the Hamiltonian.[5,6] We have previously developed a model[7] that combines the Jahn−Teller E⊗e potential energy surface of an isolated six-coordinate copper(II) complex with a lower symmetry potential due to the site symmetry of the host lattice. This approach is appropriate for isolated complexes in which the interactions between copper(II) centers are minimized, in particular, for copper(II) complexes doped into diamagnetic host crystals at low concentrations.

In this model, the potential energy surface is parametrized and the vibronic energy levels and wave functions can be obtained, from which electronic properties such as *g* values, or geometric properties such as bond lengths, can be calculated. The fitting of these properties to experiments by varying the parameters allows the ground-state potential

* Author to whom correspondence should be addressed. E-mail: m.riley@uq.edu.au.
† School of Molecular and Microbial Science, University of Queensland.
‡ Centre for Magnetic Resonance, University of Queensland.
§ University of Tasmania.
|| University of Hawaii.

(1) Murphy, B.; Hathaway, B. *Coord. Chem. Rev.* **2003**, *243*, 237.
(2) Liehr, A. D.; Ballhausen, C. J. *Ann. Phys.* **1958**, *3*, 304.
(3) Longuet-Higgins, H. C.; Öpik, U.; Pryce, M. H. L.; Sack, R. A. *Proc. R. Soc. London, Ser. A* **1958**, *A244*, 1.
(4) O'Brien, M. C. M. *Proc. R. Soc. London, Ser. A* **1964**, *A281*, 323.
(5) Ham, F. S. JTE in EPR spectra. In *Electron Paramagnetic Resonance*; Geschwind, S., Ed.; Plenum Press: New York, 1972; pp 1.
(6) Englman, R.; Halperin, B. *Phys. Rev. B: Condens. Matter Mater. Phys.* **1970**, *2*, 75.
(7) Riley, M. J.; Hitchman, M. A.; Mohammed, A. W. *J. Chem. Phys.* **1987**, *87*, 3766.

10.1021/ic8007206 CCC: $40.75
Published on Web 08/09/2008

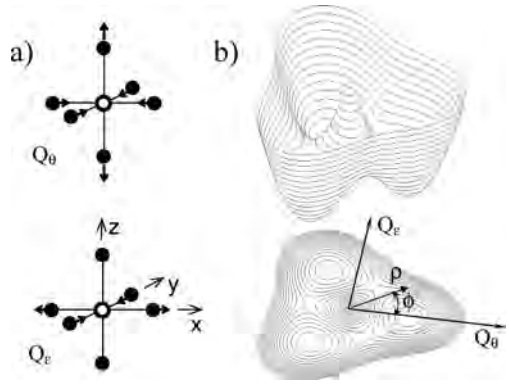

Figure 1. (a) The tetragonal (Q_θ) and orthorhombic (Q_ε) components of the Jahn−Teller-active e_g vibration of an ML_6 complex in terms of atomic displacements along molecular *x*, *y*, and *z* axes. (b) The E⊗e Jahn−Teller surface as a function of the Q_θ and Q_ε vibrational coordinates, which can also be defined in terms of the polar coordinates ρ, ϕ.

energy surface to be quantified. Often, the exchange between the thermally populated vibronic levels is much faster than the time scale of an electron paramagnetic resonance (EPR) experiment, while the X-ray structure determination yields the weighted average of the metal−ligand bond lengths, so that the observed properties are a simple thermal average of the properties of the populated vibronic levels. On the other hand, vibronic levels that are strongly localized in different minima that are separated by a large energy barrier may have slower exchange rates, resulting in a superposition, rather than the average, of the properties of the individual levels being observed. Often, a temperature-dependent exchange rate will result in different (and sometimes overlapping) temperature regions of both superimposed and averaged EPR spectra.[8]

Particular types of potential energy surfaces can result in energetically low-lying vibronic levels that have very different electronic and geometric properties. These result in a potential energy surface which gives rise to a marked temperature dependence of the electronic and geometric properties, and the present study is of a compound which displays this behavior. For isolated six-coordinate copper(II) complexes involving identical ligands, the E⊗e Jahn−Teller effect results in the three equivalent minima shown in Figure 1, corresponding to a distortion along the Q_θ, or tetragonal, component of the Jahn−Teller active e_g vibration and the two equivalent tetragonal distortions from the permutation of the *x*, *y*, and *z* axes. The sign of the distortion is such that these minima are at tetragonally elongated rather than compressed geometries, and this sign has been found to be principally determined by anharmonicity effects and 3d−4s mixing.[9−11] The symmetry of such a potential energy surface is such that the minima are at the same energy, but the substitution of a $Cu^{II}L_6$ complex into a host lattice at a site with lower than octahedral symmetry will result in the $Cu^{II}L_6$ complex being trapped in just one of the three minima. The geometry of the molecule in its lowest vibronic level is then strongly localized at this particular tetragonally elongated geometry. Higher vibronic levels can be (i) more delocalized within the same minimum, (ii) delocalized over more than one minimum, or (iii) localized at the geometry of a higher energy minimum, and the geometric and electronic properties of the complex become temperature-dependent.

If the host crystal imposes a strong tetragonal compression, it can force the $Cu^{II}L_6$ complex to also adopt a compressed geometry. However, for the potential energy surface to have a minimum at the compressed geometry, it must overcome the intrinsic E⊗e potential energy surface that has a saddle point at this geometry. This results in a decreased curvature, or softening of the potential energy surface, along the direction of the Q_ε component of the Jahn−Teller active vibration. For a $Cu^{II}L_6$ complex, the resulting low-energy, large amplitude, vibronic levels will have different vibronic mixtures of the d_{z^2} and $d_{x^2-y^2}$ orbitals and will show a large temperature dependence of the EPR spectrum. This situation is realized, for example, in Cu(II)-doped K_2ZnF_4[12] where the *g* values of the CuF_6^{4-} complex are typical of a d_{z^2}-type electronic state in a compressed geometry, but with a marked temperature dependence.

A situation which is more common in practice is where the host crystal has a lower than tetragonal symmetry, for example, the C_i site in Tutton's salts of the general formula $(cation)_2Zn(H_2O)_6(SO_4)_2$.[7] The rhombic symmetry can be broken down into tetragonal (S_θ) and orthorhombic (S_ε) components of the strain imposed by the host site. If the tetragonal component is a compression (negative S_θ), it will lower two of the Jahn−Teller minima with respect to the third, and the orthorhombic component will then discriminate between the two lower minima. Depending on the size of the orthorhombic component, temperature-dependent *g* values will then be observed as the higher of the two minima becomes thermally populated. Both these two lowest-energy minima will have an orthorhombic geometry; the positions of the minima change from values of $\phi = 120$ and 240° in Figure 1b (corresponding to tetragonal elongations along *x* and *y*, respectively) to orthorhombic distortions with the angle ϕ of the minima positions shifted toward 180°. At low temperatures, the *g* values will be those of the lowest orthorhombic minimum, while at higher temperatures with fast exchange, the *g* values will be the Boltzmann weighted average of the *g* values in each of the two lower minima. The model that we have developed involves solving the Jahn−Teller Hamiltonian of coupled vibronic equations, though the conclusions reached are often very similar to the "two-site" model used in the earlier work of Silver and Getz.[13] The two-site model rationalizes the temperature dependence of the *g* values as a thermal equilibrium between two Jahn−Teller configurations of the $Cu^{II}L_6$ complex, with identical *g* values but for which the directions of the highest and intermediate *g* values are interchanged. When comparing

(8) Riley, M. J.; Hitchman, M. A.; Reinen, D.; Steffen, G. *Inorg. Chem.* **1988**, *27*, 1924.
(9) Deeth, R.; Hitchman, M. A. *Inorg. Chem.* **1986**, *25*, 1225.
(10) Riley, M. J. *Inorg. Chim. Acta* **1998**, *268*, 55.
(11) García-Fernández, P.; Bersuker, I. B.; Aramburu, J. A.; Barriuso, M. T.; Moreno, M. *Phys. Rev. B: Condens. Matter Mater. Phys.* **2005**, *71*, 184117.
(12) Riley, M. J.; Hitchman, M. A.; Reinen, D. *Chem. Phys.* **1986**, *102*, 11.
(13) Silver, B.; Getz, D. *J. Chem. Phys.* **1974**, *61*, 638.

the two-site and vibronic models, to a good approximation, the two conformations correspond to particular vibronic levels that are strongly localized at different minima, and the energy separation and g values of these vibronic levels correspond closely to those that would be obtained from the two-site model.

The strength of the vibronic model, however, is that it rationalizes this type of temperature-dependent behavior in terms of the low-symmetry contributions of the host lattice, and indeed one can use the Cu^{II} ion as a probe of the host lattice structure. The vibronic model has successfully been used to interpret the temperature dependence of the EPR spectra of Cu(II) doped into a range of host lattices[8,14−16] and extended to treat the concomitant variations in the copper−ligand bond lengths observed for several pure copper(II) compounds.[17−20] This model has also been applied to other related Jahn−Teller systems such as Mn(III).[21] It should also be noted that there are many examples of Cu(II) systems with temperature-dependent EPR spectra that successfully interpret their data in terms of the Silver and Getz model.[1,22−24]

Here, we report a study of the temperature dependence of the EPR spectrum of ∼1% Cu(II) doped into the compound $Ba_2Zn(HCO_2)_6\cdot 4H_2O$. This follows earlier studies of this system which identified temperature-dependent g values as being due to fast exchange between different Jahn−Teller distortions of the $Cu^{II}O_6$ group.[25,26] A more recent single-crystal X-band EPR and electron spin echo study[27] has applied the Silver and Getz model[13] to interpret the temperature-dependent g values and concluded that the energy gap of a two-site model varies with the temperature. This is surprising, as it implies that there may be cooperative interactions which would not be expected for a dilute sample or that the strain induced by the lattice varies with the temperature. This has prompted us to measure the EPR spectra at Q-band frequencies and to fit the data in terms of the multilevel vibronic model. This approach has the advantage that the strain parameters can be used to estimate the geometry of the host crystal. We have also redetermined the crystal structure of the $Ba_2Zn(HCO_2)_6\cdot 4H_2O$ host and compared the $Zn^{II}O_6$ geometry with that predicted by the strain parameters derived from the analysis of the EPR spectra of the Cu^{II} ion doped into this lattice.

Experimental Section

Preparation of Compounds. Single crystals of $Ba_2Zn(HCO_2)_6\cdot 4H_2O$ were grown by slow evaporation of an aqueous solution containing a stoichiometric mixture of barium formate and zinc formate dihydrate. The Cu(II)-doped crystals were obtained from the evaporation of the above aqueous solutions with 1% copper formate tetrahydrate.

EPR Measurements. EPR measurements were carried out at Q-band (∼34 GHz) in the temperature range 100−360 K using a Bruker ESP3000E spectrometer. The temperature was controlled by an Oxford Instruments ITC504 and a nitrogen flow cryostat. The microwave frequency and magnetic field were calibrated by an EIP845B microwave frequency counter and a Bruker ER035 M gauss meter. Powdered samples were used and the data analyzed by an in-house powder simulation program.

Results and Discussion

The Structure of $Ba_2Zn(HCO_2)_6\cdot 4H_2O$. The crystal structure of $Ba_2Zn(HCO_2)_6\cdot 4H_2O$ at room temperature, illustrated in Figure 2, belongs to the triclinic space group $P\bar{1}$ and is isomorphic with those in the series $Ba_2M(HCO_2)_6\cdot 4H_2O$ (M = Co, Ni, Cu).[28] The $Zn(HCO_2)_6^{4-}$ ion in $Ba_2Zn(HCO_2)_6\cdot 4H_2O$ lies on an inversion center with small differences in the three independent Zn−O distances (Table 1), similar to the Zn(II) Tutton's salts (also given in Table 1). An earlier structural study[29] suggested that the Zn ion was coordinated to four formate ions and two water molecules, so we redetermined the crystal structure for this compound and found essentially the same results as given by Baggio et al.,[28] confirming that the Zn ion is coordinated to the oxygen atoms from six formate ions. The present system offers a significant spectroscopic advantage in that there is a single ion in the unit cell, while in the monoclinic space group of the Tutton's salts series, the two symmetry-related ions in the unit cell result in overlapping EPR spectra with the axes along the long and medium bonds approximately perpendicular. The crystal structure of a single crystal of $Ba_2Zn(HCO_2)_6\cdot 4H_2O$ with ∼1% Cu(II) doping was also solved, which was shown to retain the host structure.

In a study of the isomorphic series $Ba_2M(HCO_2)_6\cdot 4H_2O$ (M = Co, Ni, Cu, Zn), it was found that, while the Cu compound was the only one with large deviations from the average M−O bond length, they all showed small deviations with the same short, medium, and long bonds along the M−O1A, M−O2B, and M−O1C bonds, respectively.[28] Consideration of the packing arrangement shows a very high connectivity of the three unique formate ions (labeled A, B, and C). Both oxygen atoms on each formate ion form two

(14) Steffen, G.; Reinen, D.; Stratemeier, H.; Riley, M. J.; Hitchman, M. A.; Mathies, H.; Recker, K.; Wallrafen, F.; Niklas, J. R. *Inorg. Chem.* **1990**, *29*, 2123.
(15) Headlam, H.; Hitchman, M. A.; Stratemeier, H.; Smits, J. M. M.; Beurskens, P. T.; Boer, E. d.; Janssen, G.; Gatehouse, B. M.; Deacon, G. B.; Ward, G. N.; Riley, M. J.; Wang, D. *Inorg. Chem.* **1995**, *34*, 5516.
(16) Massa, M. B.; Dalosto, S. D.; Ferreyra, M. G.; Labadie, G.; Calvo, R. *J. Phys. Chem. A* **1999**, *103*, 2606.
(17) Bebendorf, J.; Bürgi, H. B.; Gamp, E.; Hitchman, M. A.; Murphy, A.; Reinen, D.; Riley, M. J.; Stratemeier, H. *Inorg. Chem.* **1996**, *35*, 7419.
(18) Simmons, C. J.; Hitchman, M. A.; Stratemeier, H.; Schultz, A. J. *J. Am. Chem. Soc.* **1993**, *115*, 11304.
(19) Hitchman, M. A.; Maaskant, W.; Plas, J. v. d.; Simmons, C. J.; Stratemeier, H. *J. Am. Chem. Soc.* **1999**, *121*, 1488.
(20) Simmons, C. J.; Stratemeier, H.; Hitchman, M. A.; Riley, M. J. *Inorg. Chem.* **2006**, *45*, 1021.
(21) Tregenna-Piggott, P. L. W. *Inorg. Chem.* **2008**, *47*, 448.
(22) Goslar, J.; Wencka, M.; Lijewski, S.; Hoffmann, S. K. *J. Phys. Chem. Solids* **2006**, *67*, 2614.
(23) Augustyniak-Jabłokow, M. A.; Usachev, A. E. *J. Phys.: Condens. Matter* **1999**, *11*, 4391.
(24) Hoffmann, S. K.; Goslar, J.; Hilczer, W.; Augustyniak-Jabłokow, M. A. *J. Phys.: Condens. Matter* **2001**, *13*, 707.
(25) Reddy, T. R.; Srinivasan, R. *Phys. Lett.* **1966**, *22*, 143.
(26) Schlick, S.; Getz, D.; Silver, B. *Chem. Phys. Lett.* **1975**, *31*, 555.
(27) Idziak, S.; Goslar, J.; Hoffmann, S. K. *Mol. Phys.* **2004**, *102*, 55.
(28) Baggio, R.; Stoilova, D.; Polla, G.; Leyva, G.; Garland, M. T. *J. Mol. Struct.* **2004**, *697*, 173.
(29) Sundara Rao, R. V. G.; Sundaramma, K.; Sivasankra Rao, G. *Z. Kristallogr.* **1958**, *110*, 231.

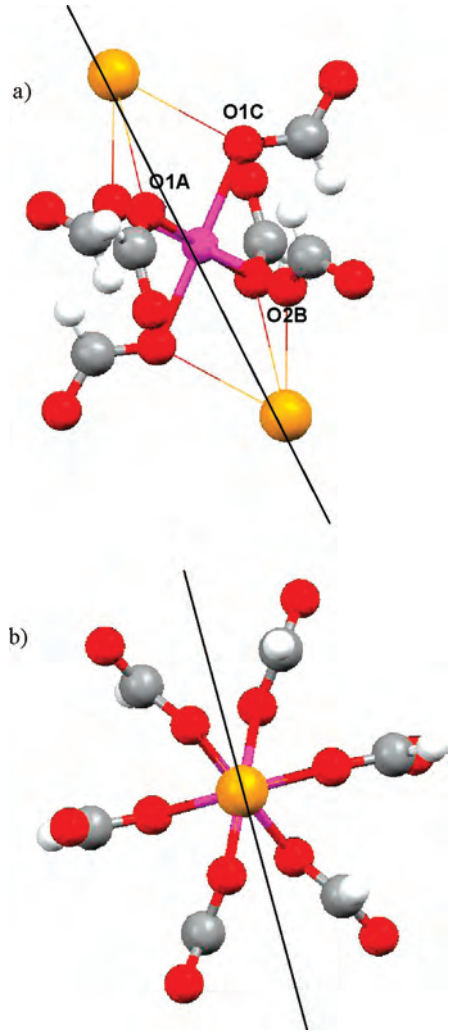

Figure 2. Structural diagrams of the $[Zn(HCO_2)_6]^{4-}$ ion in $Ba_2Zn(HCO_2)_6 \cdot 4H_2O$ showing (a) pseudo-trigonal and (b) pseudo-2-fold axes. The numbering of the coordinated oxygens follows that of the structure.

strong bonds to the cations (Ba^{2+} and/or M^{2+}) apart from the oxygens: O2A (which forms a single bond to a Ba^{2+} ion and a hydrogen bond to a water molecule) and O2C (which has only three hydrogen bonds). The 10-coordinate Ba polyhedra form chains parallel to the *b* crystal axis with the M octahedra bridging between these chains as shown in Figure 2a.[28]The positions of the formate ions are then highly constrained, with formate C being the least constrained, as the O2C oxygen has only relatively weak hydrogen bonds. The fact that M−O1C is the longest bond, not only for the Cu complex but also for the non Jahn−Teller active metal ions, shows that there is an intrinsic low-symmetry environment at the metal site which is due to the packing arrangement of the lattice beyond the immediate coordination sphere.

EPR Spectra. The temperature-dependent EPR spectrum of Cu(II)/$Ba_2Zn(HCO_2)_6 \cdot 4H_2O$ at Q-band frequencies is shown in Figure 3a. The direction corresponding to the largest *g* value, $g_{max} = 2.392$ at 100 K, is parallel to the Zn−O1C bond (the longest in the $Zn(HCO_2)_6^{4-}$ complex, see Table 1). The directions associated with the intermediate and smallest *g* values are parallel to the medium and shortest Zn−O bonds, respectively. Previous single-crystal EPR measurements[27] have established that the **g** and **A** tensors are collinear and that their principal directions are temperature-independent over the 4−300 K temperature range. At low temperatures, the spectrum is of a system with a **g** tensor of near axial symmetry, with $g_{\|} > g_{\perp}$. This is characteristic of an electronic ground-state with the electron hole of the d^9 Cu(II) electron configuration in the x^2-y^2 d orbital, as expected for a six-coordinate Cu(II) ion in a tetragonally elongated geometry. In anticipation of the analysis that follows, we denote the maximum, intermediate, and lowest *g* values as g_x, g_y, and g_z, respectively. This at first appears to be an unusual choice but results from the *z* axis being defined as the direction of the principal component of the lattice strain.[2] Hyperfine structure due to coupling with the copper nuclear spin $I = {}^3/_2$ is observed on the resonances due to the highest and lowest *g* values at low temperatures. As the temperature is raised, the low-field resonance corresponding to g_x and the resonance due to the g_y value broaden and start to converge. At lower temperatures, the *g* values do not vary significantly.[26,27] The thermal behavior of the EPR spectrum of $Ba_2Zn[Cu](HCO_2)_6 \cdot 4H_2O$ has some features in common with those reported for the Cu(II)-doped Tutton's salts,[7,8] which also show a smooth convergence of the two higher *g* values in the temperature range 100−300 K, with the signals progressively broadening as the temperature rises.

The lowest *g* value of the $Cu(H_2O)_6^{2+}$ ion in the Tutton's salt host does not change below ∼300 K because the lattice strain interaction has a large negative component (corresponding to a compression of the octahedral site) acting along one of the metal−ligand bond directions, so that the vibronic wave function corresponding to the axial elongation of the bonds along this direction is too high in energy to be thermally populated at room temperature.[7,13] The low-temperature *g* values are then due to only the lowest minimum (marked as **1** in Figure 4b) being occupied. The convergence of the two higher *g* values is due to the thermal population of the vibronic wave function that is localized largely in the second minimum (**2**; Figure 4b) of the warped Mexican hat potential energy surface, with the rate of exchange between the wave functions always being rapid on the EPR time scale so that the observed signal corresponds to an average of the EPR spectrum of the two levels weighted by their relative thermal populations.[13]

The most important factor deciding the thermal behavior of the EPR spectrum of the $Cu^{II}O_6$ centers in these lattices is the influence of the host lattice, in particular the magnitude of the strain interactions which perturb the warped Mexican hat potential energy surface and discriminate energetically between the directions along which the JT distortion can occur. For $Ba_2Zn[Cu](HCO_2)_6 \cdot 4H_2O$, these interactions are only slightly weaker than those in the Tutton's salts and much larger than the smaller low-symmetry lattice strains present, for example, in the $Zn(H_2O)_6XF_6$ (X = Si, Zr) lattices.[30−32]

The values of the lattice strains are reflected in the distortions exhibited by the $Zn^{II}O_6$ octahedra in the host

Table 1. Structural Parameters of the ZnO_6 Host Lattices[a]

	$Ba_2Zn(HCO_2)_6\cdot 4H_2O$		$K_2Zn(H_2O)_6(SO_4)_2$	$Rb_2Zn(H_2O)_6(SO_4)_2$	$Cs_2Zn(H_2O)_6(SO_4)_2$
Zn−O1C/Å	2.125 (2.330)[a]	Zn−O7/Å	2.1224 (2.029)	2.112 (2.000)	2.099 (2.005)
Zn−O2B/Å	2.103 (2.016)	Zn−O8/Å	2.1336 (2.312)	2.125 (2.317)	2.126 (2.312)
Zn−O1A/Å	2.073 (1.972)	Zn−O9/Å	2.0287 (1.942)	2.040 (1.978)	2.056 (1.965)
T/K	293 (293)		120 (85)	293 (77)	293 (RT[b])
r_{av}/Å	2.100 (2.106)		2.095 (2.094)	2.092 (2.098)	2.094 (2.094)
ρ_0/Å	0.052 (0.390)		0.115 (0.387)	0.092 (0.379)	0.071 (0.378)
ref	28		20, 42	43, 44	45, 46

[a] The data in parentheses are for the analogous copper structures. [b] The room temperature structure of the Cu compound is likely to show some averaging of medium and long bonds.

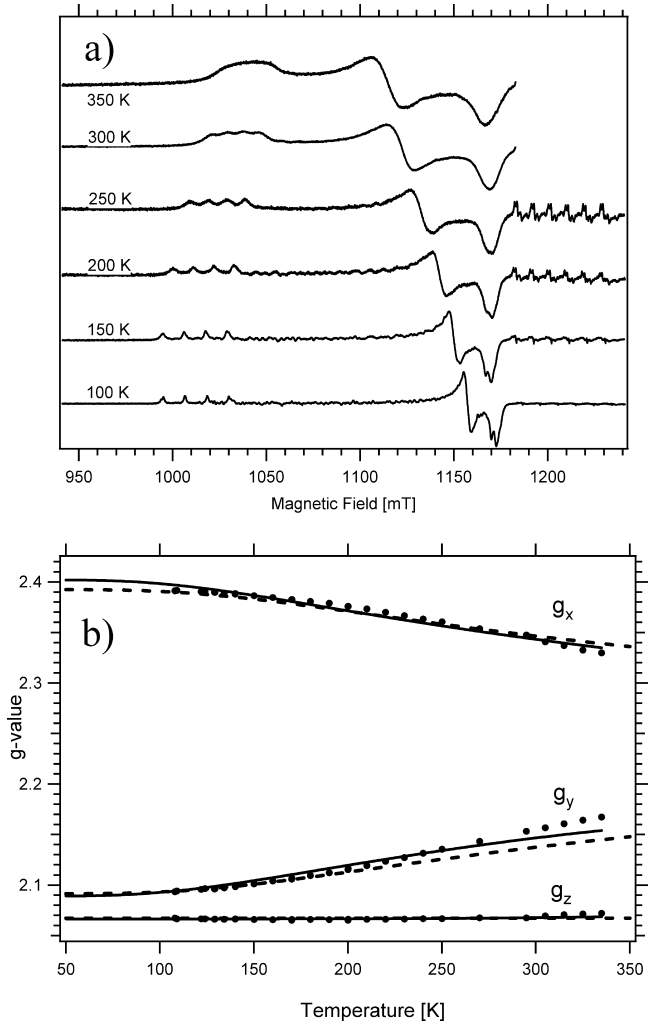

Figure 3. (a) The Q-band EPR spectrum of powdered Cu(II)/$Ba_2Zn(HCO_2)_6\cdot 4H_2O$ at various temperatures. Microwave frequency ~ 34 GHz (see Supporting Information). The resonances in the region 1180−1240 mT arise from Mn(II) impurities in the quartz EPR tubes. (b) The temperature dependence of the principal g values. The g values have been fitted to two-site (dashed) and three-site (solid) Silver and Getz models. The parameters are (two-site) $g_{x1} = 2.392$, $g_{y2} = 2.093$, $g_{z3} = 2.067$, $\Delta E_{12} = 340$ cm^{-1}; (three-site) $g_{x1} = 2.402$, $g_{y1} = 2.089$, $g_{z1} = 2.066$, $\Delta E_{12} = 310$ cm^{-1}, $\Delta E_{13} = 1125$ cm^{-1}.

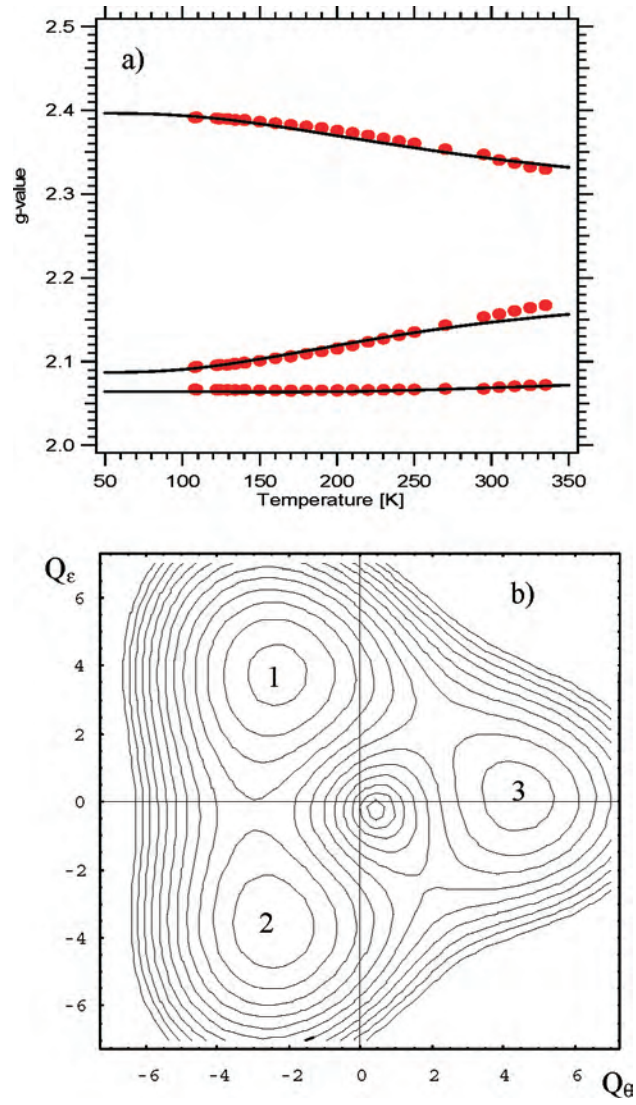

Figure 4. (a) Fit of the g values calculated from the vibronic wave functions using the potential energy surface given by the parameters $A_1 = 945$ cm^{-1}, $A_2 = 27$ cm^{-1} ($\beta = 352$ cm^{-1}), h$\nu = 267$ cm^{-1}, $S_\theta = -400$ cm^{-1}, $S_\varepsilon = 200$ cm^{-1}; $k = 0.82$, $\Delta = 12\,000$ cm^{-1}, $A_1(T_2) = 300$ cm^{-1}. (b) The lower Jahn−Teller potential energy surface using the above parameters. The minima **1**, **2**, and **3** are labeled from lowest to highest in energy. The contour interval is 200 cm^{-1}.

lattices. These are conveniently measured by the parameter ρ used to describe the JT radius of distortion of a six-coordinate copper(II) complex:[33,34]

$$\rho = \sqrt{2\Delta r_x + 2\Delta r_y + 2\Delta r_z} \qquad (1)$$

where Δr_i is the deviation of the bond lengths along the ith axis from their mean value. For $Ba_2Zn(HCO_2)_6\cdot 4H_2O$, $\rho =$ 0.052 Å, while for zinc(II) Tutton's salts, ρ lies in the range 0.071−0.119 Å (Table 1),[35] and in a system with smaller distortions such as $Cs_2Zn(H_2O)_6(ZrF_6)_2$, it is only 0.009 Å.[32] All of these values are small compared to those of pure copper(II) complexes; for $Ba_2Cu(HCO_2)_6\cdot 4H_2O$, one finds $\rho = 0.390$ Å.[28] Thus, the low-symmetry perturbation of the Zn lattice acting on the Cu(II) dopant is small compared to the large intrinsic ρ of the Jahn−Teller surface shown in Figure 1b. The EPR spectrum may be used to estimate the

lattice interactions perturbing the copper(II) complex, as discussed below, though these may differ somewhat from those acting on the $Zn^{II}O_6$ center because of the different shapes of the copper and zinc complexes.

Potential Energy Surface of the Copper(II) Complex. The "warped" Mexican hat potential energy surface that results from the perturbation of a Jahn−Teller E⊗e potential for a six-coordinate copper(II) complex by interactions with the surrounding lattice has been discussed extensively.[6,33,36] The basic parameters defining the E⊗e potential energy surface of a six-coordinate $Cu^{II}O_6$ center in the absence of lattice perturbations typically take the values[7] $A_1 = 900$ cm^{-1}, $h\nu_{JT} = 300$ cm^{-1}, and $\beta = \sim 300$ cm^{-1}.

These values have been used to interpret successfully the temperature dependence of the **g** tensors observed for the $Cu(H_2O)_6^{2+}$ complex ion in a range of zinc(II) Tutton's salts[7] and were therefore taken as the starting point in the present calculations. Here, A_1 is the linear Jahn−Teller coupling constant and $h\nu_{JT}$ is the energy of the Jahn−Teller active vibration, both known quite accurately from spectroscopic studies.[7] However, the parameter β, which describes the energy by which the minima of the basic warped Mexican hat potential energy surface are stabilized by higher-order effects, is much less well-defined, as it is an effective parameter that contains contributions from second-order Jahn−Teller coupling, vibrational anharmonicity, and 3d−4s mixing.[9,10] We do not actually use cubic terms from the vibrational anharmonicity in the vibronic Hamiltonian,[11] as we have found that they cause numerical instabilities at the required large vibronic basis sizes,[7] and a particular value of β is obtained from adjusting the second-order coupling constant A_2.

The temperature dependence of the g values is due to the perturbation of the potential energy surface by lattice interactions, which are represented by the axial and orthorhombic strain components S_θ and S_ε, which render the three minima of the warped Mexican hat potential energy surface inequivalent. Provided that the strain is small compared with β, it has little effect on the position of the minima in the potential energy surface. The energy of the highest well relative to the lowest is determined largely by S_θ, while that of the intermediate well is influenced mainly by S_ε. Provided that the warping of the potential energy surface is relatively large, it follows that the temperature dependence of the highest and intermediate g values depends mainly upon S_ε, while that of the lowest g value is determined largely by S_θ.[7,37] When $S_\theta < 0$, the ratio of β to S_θ strongly influences the position of the lowest-energy minimum in the warped Mexican hat potential energy surface, and hence the anisotropy of the g values of the lowest vibronic wave function.[7,36,38,39] This means that, if the axial strain is well-defined, the warping parameter may be deduced accurately also.

The above constraints were used to fit the g values of $Ba_2Zn[Cu](HCO_2)_6 \cdot 4H_2O$ over the whole temperature region, and good agreement with experimental results (Figure 4a) was obtained using the warping and strain parameters: $\beta = 350$ cm^{-1}, $S_\theta = -400$ cm^{-1}, and $S_\varepsilon = 200$ cm^{-1}.

Here, the negative sign for S_θ means that the strain acts as a tetragonal compression. The g values were calculated for each separate vibronic level, which assumes that they are far enough apart so that the magnetic field acts as a small perturbation. The calculation requires the results from the vibronic calculation (2652×2652 diagonalization for a n_{vib}=50 basis) used in a 10×10 ligand field diagonalization which includes spin−orbit coupling. The excited T_{2g} states are described by a mean energy $E(^2T_{2g}) = 10\,000$ cm^{-1} and a linear coupling constant of the excited state $A_1(^2T_{2g}) = -500$ cm^{-1}. An orbital reduction parameter $k = 0.81$ was used to calculate the g values from the electronic components of the vibronic wave functions. These values are quite similar to those giving optimum agreement with the experimental data of the Cu^{2+}-doped Tutton's salts[7] ($E(^2T_{2g}) = 11\,900$ cm^{-1}, $A_1(^2T_{2g}) = -330$ cm^{-1}, $k = 0.88$). In common with the doped Tutton's salts, the lowest g value shows little temperature dependence, so that the axial strain, and hence the warping parameter β, could only be estimated rather approximately.[7]

The warped Jahn−Teller potential energy surface given by the fitted parameters is shown in Figure 4b. The inequivalence of the three minima (marked as **1**−**3** in order of increasing energy) caused by the low-symmetry strain terms S_θ and S_ε formally make the E⊗e surface an (A⊕B)⊗(a⊕b) problem. However, we retain the high-symmetry constants. The a and b vibrational modes which are formally nondegenerate in this low symmetry are still described by a single harmonic vibrational wavenumber, $h\nu$, and a single first-order Jahn−Teller coupling constant A_1 is used.

Vibronic Wave Functions. A useful picture of the structures involved in the dynamic behavior is provided by the probability plots of the vibrational and electronic parts of the vibronic wave functions as a function of the two vibrational coordinates Q_θ and Q_ε. These are shown in Figure 5 for the first five levels, together with their energy, as calculated using the fitted potential parameters given in Figure 4b. The three lowest levels are each strongly localized in the lowest energy minimum of the warped potential energy surface (marked **1** in Figure 4b). To a good approximation, the second and third levels correspond to the first excited vibrational level (approximately doubly degenerate) in this minimum, with a node in the Q_θ and Q_ε directions. The fourth wave function plot is localized at the first excited minimum

(30) Dang, L. S.; Buisson, R.; Williams, F. I. B. *J. Phys. (Paris)* **1974**, *35*, 49.
(31) Ziatdinov, A. M.; Zaripov, M. M.; Yablokov, Y. V.; Davidovich, R. L. *Phys. Status Solidi B* **1976**, *78*, K69.
(32) Hitchman, M. A.; Yablokov, Y. V.; Petrashen, V. E.; Augustyniak-Jablokov, M. A.; Stratemeier, H.; Riley, M. J.; Lukaszewicz, K.; Tomaszewski, P. E.; Pietraszko, A. *Inorg. Chem.* **2002**, *41*, 229.
(33) Reinen, D.; Friebel, C. *Struct. Bonding (Berlin)* **1979**, *37*, 1.
(34) Reinen, D.; Atanasov, M. *Magn. Reson. Rev.* **1991**, *15*, 167.
(35) Simmons, C. J.; Hitchman, M. A.; Stratemeier, H. *Inorg. Chem.* **2000**, *39*, 6124.
(36) Hitchman, M. A. *Comments Inorg. Chem.* **1994**, *15*, 197.
(37) Reinen, D.; Hitchman, M. A. *Z. Phys. Chem.* **1997**, *200*, 11.
(38) Levin, A. A.; Fedorova, I. S.; D'yachkov, P. N. *Sov. J. Coord. Chem.* **1985**, *11*, 415.
(39) Reinen, D.; Krause, S. *Inorg. Chem.* **1981**, *20*, 2750.

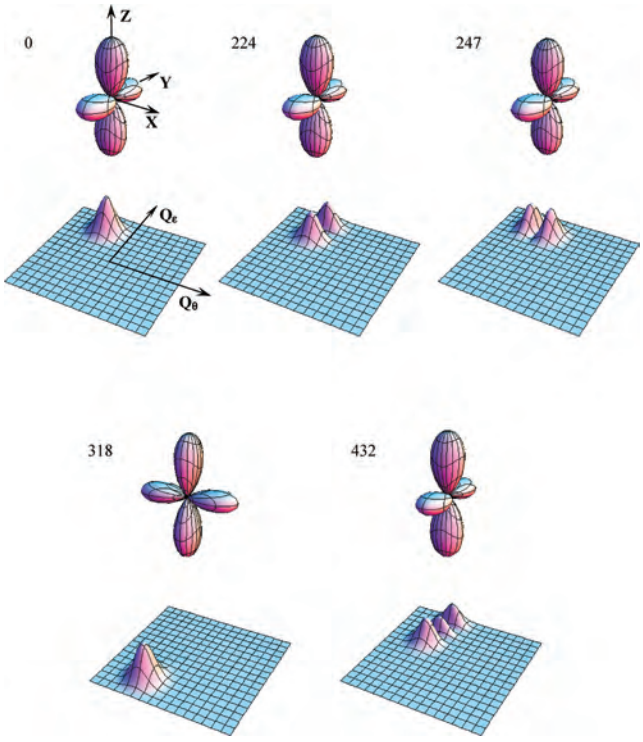

Figure 5. Plots of the probability functions of the lowest four vibronic levels in electronic and vibrational space, for the potential energy surface given in Figure 4b. The energies are in cm^{-1}.

Table 2. The Calculated g Values of the First Five Vibronic Levels

level	energy/cm^{-1}	g_x	g_y	g_z
1	0	2.3964	2.0869	2.0642
2	224	2.3996	2.0984	2.0580
3	247	2.4038	2.0828	2.0713
4	318	2.1030	2.4041	2.0536
5	432	2.3947	2.1189	2.0486

(**2** in Figure 4b). The fifth level is again predominantly localized in the lowest minimum; by counting the nodes, it is the second excited vibrational state in the Q_ε direction. It can be noted that in general the vibrational parts of the wave functions remain nearly pure Q_θ and Q_ε components, rather than the angular and radial modes that occur when the low-symmetry strain terms are small.[32] Although it cannot be seen on the scale of the plots, the highest-energy vibrational level near the barrier height between the minima is more delocalized over both minima and provides a relaxation pathway between the minima.

The electronic probability functions of the electron hole of the d^9 system provide a similar perspective. For the three lowest levels, the electronic probability function is a "y^2-z^2 type" orbital that would be expected for a Cu(II) complex elongated along the x axis, while the fourth level is a "z^2-x^2 type" orbital typical of an elongation along the y axis. Although it cannot be seen on the scale of the figure, the fifth level is of a more delocalized nature, having a small probability lobe along the x axis. The nature of the electronic components of the vibronic functions is reflected in their g values, and those of the first five levels are given in Table 2. It is important to remember that these very different electronic and geometric properties are for different vibronic levels of a single metal site. The temperature-dependent behavior arises from the thermal population of energy levels of a single site rather than an equilibrium between different sites with different electronic properties.

The influence of lattice strain on the position and relative energies of the minima in the JT surface has been discussed in detail elsewhere.[36,39] When such strain interactions are small, the higher-order terms which warp the potential energy surface, parametrized by β, favor minima at $\phi = 0°$, 120°, and 240°, each of which corresponds to a tetragonally elongated octahedral geometry. An axial compression shifts the minima from these positions, and it has been shown that the ratio $|S_\theta/\beta|$ must exceed 9 for the lowest-energy minimum to correspond to a compressed tetragonal geometry.[39] When $|S_\theta/\beta| < 9$, an orthorhombic geometry and **g** tensor occur. In the present case, $S_\theta = -400\ cm^{-1}$ and $\beta = 352\ cm^{-1}$, so the ratio, 1.2, is small and the orthorhombic distortion away from the $\phi = 120°$ tetragonal elongation position associated with the lowest vibronic wave functions is also small.

Relation to the Silver and Getz Model. Previous interpretations of the dynamic behavior of copper(II) complexes have often involved an equilibrium between two "orientation isomers" which have identical g values and bond lengths, but with the directions of the largest and intermediate g values interchanged, as originally proposed by Silver and Getz.[13] This approach has been used to interpret the temperature dependence of the two higher g values[17,27] and metal−ligand bond lengths[40] of a range of complexes. Expressions for the two-site Silver and Getz model for the temperature-dependent g values of the complex are given by[7,13,41]

$$\begin{aligned} g_x(T) &= K_1 g_{x1} + K_2 g_{y1} \\ g_y(T) &= K_1 g_{y1} + K_2 g_{x1} \\ g_z(T) &= K_1 g_{z1} + K_2 g_{z1} = g_{z1} \end{aligned} \qquad (2)$$

Here, K_i is the fractional population in level i determined by a Boltzmann population and g_{x1}, g_{y1}, and g_{z1} are the g values of the lowest level, where the subscripts z, y, and x refer to the g values along the shortest, middle, and longest Cu−O bonds, respectively, for the lowest level. As discussed previously,[13] this choice of a molecular coordinate system results from the fact that the principal symmetry axis of the system is provided by the axial strain resulting in the lowest minimum of the potential energy surface at $\phi = \sim 120°$ in Figure 4b. In the two-site Silver and Getz model, the g_x and g_y of level 2 are just the g_{y1} and g_{x1}, respectively, of the lowest level. Equation 2 then suggests that, given the g values at low temperatures, their temperature dependence depends on just a single parameter, ΔE_{12}, the relative energy of level

(40) Simmons, C. *New J. Chem.* **1993**, *17*, 77.
(41) Petrashen, V. E.; Yablokov, Y. V.; Davidovitch, R. L. *Phys. Status Solidi B* **1986**, *101*, 117.
(42) Simmons, C. J. Unpublished data.
(43) Euler, H.; Barbier, B.; Klumpp, S.; Kirfel, A. *Z. Kristallogr. NCS* **2000**, *215*, 473.
(44) Smith, G.; Moore, F. H.; Kennard, C. H. L. *Cryst. Struct. Commun.* **1975**, *4*, 407.
(45) Euler, H.; Barbier, B.; Meents, A.; Kirfel, A. *Z. Kristallogr. NCS* **2003**, *218*, 409.
(46) Ballirano, P.; Belardi, G.; Bosi, F. *Acta Crystallogr., Sect. E* **2007**, *E63*, 164.
(47) Shannon, R. D. *Acta Crystallogr., Sect. A* **1976**, *A32*, 751.

Table 3. The Zn−O Bond Lengths Calculated from the Strain Parameters for Several ZnO_6 Host Lattices

	$Ba_2Zn(HCO_2)_6\cdot 4H_2O$	$K_2Zn(H_2O)_6(SO_4)_2$	$Rb_2Zn(H_2O)_6(SO_4)_2$	$Cs_2Zn(H_2O)_6(SO_4)_2$
S_θ/cm^{-1}	−400	−1000	−800	−650
S_ε/cm^{-1}	200	55	110	200
$-\lvert S_\theta\rvert/S_\varepsilon$	2	18	7.3	3.2
radii/Å[a]		1.51	1.61	1.74
Q_θ^0/Å	−0.038	−0.094	−0.070	−0.057
Q_ε^0/Å	0.019	0.005	0.010	0.018
Δr_x/Å	0.020(0.025)[b]	0.028(0.039)	0.025(0.033)	0.025(0.032)
Δr_y/Å	0.001(0.003)	0.023(0.027)	0.015(0.020)	0.008(0.005)
Δr_z/Å	−0.022(−0.027)	−0.051(−0.066)	−0.041(−0.052)	−0.033(−0.038)

[a] Ionic radii for K^+, Rb^+, and Cs^+ taken from ref 47 for 8 coordination. [b] The bracketed Δr_i values are from the experimental X-ray structural data given in Table 1.

2 with respect to level 1. A least-squares global fit of the expression in eq 2 to the observed temperature-dependent g values of $Ba_2Zn[Cu](HCO_2)_6\cdot 4H_2O$ is shown as a dashed line in Figure 3b, giving the energy $\Delta E_{12} = 340\ cm^{-1}$. This energy gap is close to the energy of the fourth vibronic level (318 cm^{-1}) that is localized in minimum **2**. Moreover, as may be seen from Table 2, the values deduced for g_x and g_y for level 4 are interchanged compared with those of level 1, confirming that the Silver and Getz model is a good approximation for this system.

This approach has been extended into a three-site model:[32,41]

$$\begin{aligned} g_x(T) &= K_1 g_{x1} + K_2 g_{y1} + K_3 g_{y1} \\ g_y(T) &= K_1 g_{y1} + K_2 g_{x1} + K_3 g_{z1} \\ g_z(T) &= K_1 g_{z1} + K_2 g_{z1} + K_3 g_{x1} \end{aligned} \tag{3}$$

The third level of this three-site model is associated with the highest minimum on the Jahn−Teller surface. The fit shown as the solid line in Figure 3b is slightly better (as might be expected for an extra fitting parameter), giving the energy gaps $\Delta E_{12} = 310\ cm^{-1}$ and $\Delta E_{13} = 1125\ cm^{-1}$. These energies are close to those of the vibronic levels that are localized at the minima **2** and **3**, respectively (level 4, 318 cm^{-1}, and level 26, 1010 cm^{-1}); however, they do not reproduce the temperature dependence in detail. It is also noted that the three-site model is oversimplified by using the one set of g values. Although the third level would be expected to have medium, short, and long bonds along the x, y, and z axes, respectively, as implied by the labeling of the g values given in eq 3, it is not expected to be as orthorhombically distorted as levels 1 and 2. This is because the position of minimum **3** in the Jahn−Teller potential energy surface will not be shifted away from $\phi = 0°$ by the tetragonal component of the strain, S_θ, as the lower minima **1** and **2** are shifted from 120° and 240°, respectively.[39] The three-site model is better suited to systems of small tetragonal strain.[32]

Relation of the Low-Symmetry Strain Parameters to the Host Structure. The strain parameters (S_θ and S_ε) derived in the present approach should be related semiquantitatively to the structure of the host lattice. For the present E⊗e Jahn−Teller effect, this relationship has been given by Ham[5] as

$$\begin{aligned} S_\theta &= A_1 \alpha Q_\theta^0 \\ S_\varepsilon &= A_1 \alpha Q_\varepsilon^0 \end{aligned} \tag{4}$$

where $\alpha = 0.1722\sqrt{(Mh\nu)}\ Å^{-1}$ (=11.26 $Å^{-1}$ for M = 16 amu, $h\nu = 267\ cm^{-1}$)[17] and A_1 is the first-order Jahn−Teller coupling constant and Q_θ^0 and Q_ε^0 can be viewed as a displacement along the e_g coordinates in the absence of the Jahn−Teller effect. From Q_θ^0 and Q_ε^0, one can calculate the deviation $\Delta r_{x,y,z}$ from an average bond length using

$$\begin{pmatrix} \Delta r_x \\ \Delta r_y \\ \Delta r_z \end{pmatrix} = \begin{pmatrix} -\frac{1}{\sqrt{12}} & +\frac{1}{2} \\ -\frac{1}{\sqrt{12}} & -\frac{1}{2} \\ +\frac{2}{\sqrt{12}} & 0 \end{pmatrix} \begin{pmatrix} Q_\theta^0 \\ Q_\varepsilon^0 \end{pmatrix} \tag{5}$$

Using these equations, the parameters found from fitting the EPR spectra of the $Cu(HCO_2)_6^{4-}$ center to the vibronic model may be used to estimate the ligand displacements in the $Zn(HCO_2)_6^{4-}$ complex of the host crystal. The doped copper(II) impurity ion is thus acting as a probe of the host geometry. For the strain parameters suggested by the g values at lower temperatures, $S_\theta = -400\ cm^{-1}$ and $S_\varepsilon = 200\ cm^{-1}$, one finds

$$Q_\theta^0 = -0.038\ Å,\ Q_\varepsilon^0 = 0.019\ Å$$

which correspond to the ligand displacements

$$\Delta r_x = 0.020\ Å;\ \Delta r_y = 0.001\ Å;\ \Delta r_z = -0.022\ Å$$

The observed deviations from the mean bond length from the $Ba_2Zn(HCO_2)_6\cdot 4H_2O$ crystal structure at 293 K are

$$\Delta r_x(Zn-O1C) = 0.025\ Å;$$
$$\Delta r_y(Zn-O2B) = 0.003\ Å;$$
$$\Delta r_z(Zn-O1A) = -0.027\ Å$$

The agreement is good, and these values give an overall distortion ρ (eq 1) of 0.042 Å, which may be compared with the value of 0.052 Å observed for the zinc host at 293 K.

The strain parameters and the derived host lattice bond length distortions are given in Table 3, together with those observed for a range of related Zn Tutton's salts. Here, the strain parameters vary systematically as a function of the ionic radius of cation A in the general formula $A_2Zn(H_2O)_6(SO_4)_2$. The relationship is shown in Figure 6 together with the results for $Ba_2Zn(HCO_2)_6\cdot 4H_2O$. In every case, excellent agreement is found between the values predicted for the host bond lengths and the actual bond lengths determined from the crystal structures. The success of the model implies that the strain of the host structure is relatively temperature-independent.

For the potassium Tutton's salt on the left side of Figure 6, the strain parameters are nearly tetragonal (S_ε small; $\Delta r_x \sim \Delta r_y$). This results in a strong temperature dependence of

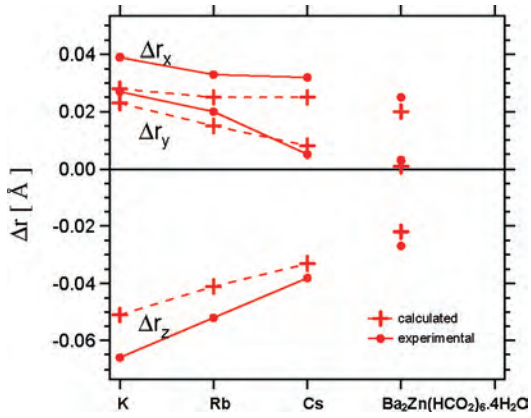

Figure 6. The experimental deviations from octahedral symmetry of the series of Cu(II)-doped Tutton's salts of general formula $X_2Zn(H_2O)_6(SO_4)_2$ and $Ba_2Zn(HCO_2)_6 \cdot 4H_2O$ compared to values obtained from fitting the temperature-dependent EPR spectrum (see Table 2) using Cu(II) as a probe.

the g values, as S_ε determines the energy separation of the two lowest minima. At room temperature, the EPR spectrum is nearly tetragonal, $g_x \sim g_y > g_z$, as the g values of these close-lying levels are averaged. For the cesium Tutton's salt, the host lattice gives a much larger orthorhombic strain, so that the EPR spectrum is less temperature-dependent and is more orthorhombic at room temperature. For the present system, the $Ba_2Zn(HCO_2)_6 \cdot 4H_2O$ host has a relatively large S_ε, but the overall strain parameters are smaller. This results in the temperature-dependent spectrum shown in Figure 3b and a significant orthorhombic component to the EPR spectra at high temperatures.

It can be noted that the lowest g value increases slightly at temperatures above 300 K, and this is correctly reproduced in the vibronic calculations as shown in Figure 4a. The reason is the comparatively low value of S_θ, which means that the vibronic level corresponding to tetragonal elongation along the z axis is slightly populated at high temperatures. Thermal decomposition is not responsible for the effect, as a thermal gravimetric analysis of $Ba_2Zn(HCO_2)_6 \cdot 4H_2O$ has shown[28] that it only starts to lose water at temperatures above 365 K. There is an abrupt change in the g values at 350 K presumably associated with a phase transition before the onset of losing water.

Conclusions

The variation of the EPR spectrum of ~1% Cu^{2+} doped into $Ba_2Zn(HCO_2)_6 \cdot 4H_2O$ can be interpreted satisfactorily using a potential energy surface given by E⊗e Jahn−Teller vibronic coupling perturbed by the strain of the host lattice. The temperature dependence of the g values and the variation of the EPR line shape with temperature both suggest that the lattice strain interactions are of a similar magnitude to those found previously for Cu(II) doped into Tutton's salts of the general formula $(cation)_2Zn(H_2O)_6(SO_4)_2$. A marked difference for the present system is a larger value for the warping parameter β that controls the barrier height between different minima. We have confirmed that the crystal structure of $Ba_2Zn(HCO_2)_6 \cdot 4H_2O$ contains Zn(II) ions on a centrosymmetric site coordinated to six formate ligands in a near octahedral arrangement, and that this structure is maintained with a small amount of added Cu(II) impurity replacing ~1% of the Zn(II) ions.

To a good approximation, the calculated lowest vibronic wave functions deduced for the $Cu(HCO_2)_6^{4-}$ ion are localized within the minima of the potential energy surface due to the large barrier heights between the minima, the energy difference to levels localized in the two lowest minima are related to the energy separations in a two-level Silver and Getz model.

At low temperatures, the EPR spectrum is that of a tetragonally elongated Cu(II) complex with a slight orthorhombic distortion, but as the temperature is raised, the high and intermediate g values are increasingly averaged as higher vibronic levels are populated. The g values vary with the temperature because of a thermal equilibrium between these vibronic energy levels. The rate of exchange between the energy levels is always fast enough that an average g value is observed in the Q-band EPR spectrum. The low symmetry strain parameters obtained from fitting the temperature-dependent EPR spectrum allowed the small departure of the $Zn(HCO_2)_6^{4-}$ ion from regular octahedral geometry to be quantified, in good agreement with the bond lengths observed in the crystal structure of $Ba_2Zn(HCO_2)_6 \cdot 4H_2O$.

Acknowledgment. We thank P.V. Bernhardt for help with the X-ray data collection.

Supporting Information Available: The fitted g and A values of the temperature-dependent EPR spectra are tabulated, together with the microwave frequency of the measurement. This material is available free of charge via the Internet at http://pubs.acs.org.

IC8007206